

# Critical exponent for the viscosity of carbon dioxide and xenon

R. F. Berg and M. R. Moldover

Thermophysics Division, National Institute of Standards and Technology, Gaithersburg, Maryland 20899

(Received 23 March 1990; accepted 27 April 1990)

The viscosities  $\eta$  of carbon dioxide and xenon have been measured near their critical points and the critical exponent  $y$  characterizing the asymptotic divergence,  $\eta \sim |T - T_c|^{-y}$ , has been determined. Both fluids yielded exponents in the range  $y = 0.041 \pm 0.001$  and thus also fell in the range  $y = 0.042 \pm 0.002$  from our earlier study of four binary liquids. This agreement between experiments is the first evidence that pure fluids and binary liquids are in the same dynamic universality class. A recent theoretical value for  $y$  is 0.032. The 30% discrepancy is much greater than the combined errors from experiment and theory. The torsion oscillator viscometer operated at low frequency and low shear rate to avoid systematic errors caused by critical slowing down. Far from  $T_c$  the analysis accounted for the crossover from critical to noncritical temperature dependence, where the latter was obtained from previously published correlations. Corrections for gravitational stratification were included close to  $T_c$ .

## I. INTRODUCTION

The renormalization group approach to critical phenomena postulates that, sufficiently near critical points, thermodynamic systems are classified by universality classes characterized by the spatial dimensionality  $d$  of the system, the number  $n$  of components of the order parameter, and whether the forces between the elements of the system are long ranged or short ranged. Pure fluids near liquid-vapor critical points and binary mixtures near consolute points are all short ranged  $d = 3$ ,  $n = 1$  systems. For these systems, the static critical exponents and the related scaling functions are well known from experiment and all are in good agreement with theory.

For dynamic properties, the universality classes for fluids must be further subdivided to account for the number of relevant hydrodynamic modes. Hohenberg and Halperin<sup>1</sup> argued that, although binary mixtures have one more hydrodynamic variable than pure fluids, their dynamic critical behavior is equivalent to that of pure fluids. In contrast, many experimental studies of the divergence of the viscosity near critical points have found smaller critical exponents for pure fluids than for binary mixtures.<sup>2</sup> This apparent conflict between the principle of universality and published data motivated the present viscosity measurements and our closely related measurements with binary mixtures.<sup>3</sup>

The present measurements near the critical points of both carbon dioxide and xenon show that the apparent critical exponent  $y$ , which characterizes the divergence of the viscosity  $\eta$  near the critical point, falls in the range

$$0.0401 < y < 0.0419. \quad (1)$$

We define  $y$  through the relation:

$$\eta \sim t^{-y}, \quad (2)$$

where  $t$  is the reduced temperature measured from the critical temperature  $T_c$ :

$$t \equiv |T - T_c|/T_c. \quad (3)$$

The present range for  $y$  falls within the wider range  $0.040 < y < 0.044$  that spans our earlier result<sup>3</sup> for four binary liquid mixtures. (See Fig. 1.) The overlap of the ranges of

$y$  is consistent with the hypothesis that binary liquid mixtures and pure fluids are in the same dynamic universality class. Although our data are consistent with universality, our values of  $y$  are significantly higher than the value 0.032 calculated with the mode coupling theory<sup>4</sup> and lead us to advocate a reexamination of the theory.

The agreement among the values of  $y$  displayed in Fig. 1 is remarkable given that the systematic errors and experimental problems encountered in determining  $y$  for pure fluids are very different than those encountered with binary liquid mixtures. We mention some of these problems now. For determining  $y$ , pure fluids are advantageous because the noncritical background viscosity has a comparatively small temperature dependence that can be more accurately characterized. This is very important because, as Fig. 2 shows, the small value of  $y$  limits the observable increase of the viscosity near  $T_c$  to only 20%–40% of the viscosity far from  $T_c$ .

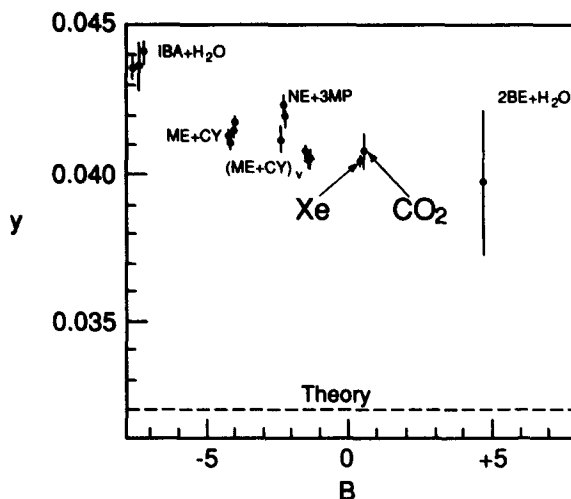


FIG. 1. The viscosity exponent  $y$  for four binary mixtures and two pure fluids. The abscissa  $B$ , defined in Eq. (36), measures the slope of the noncritical viscosity at  $T_c$ . The various fluids, chosen partly for their diverse noncritical viscosities, have exponents that agree with each other better than with the theoretical value of Ref. 4.

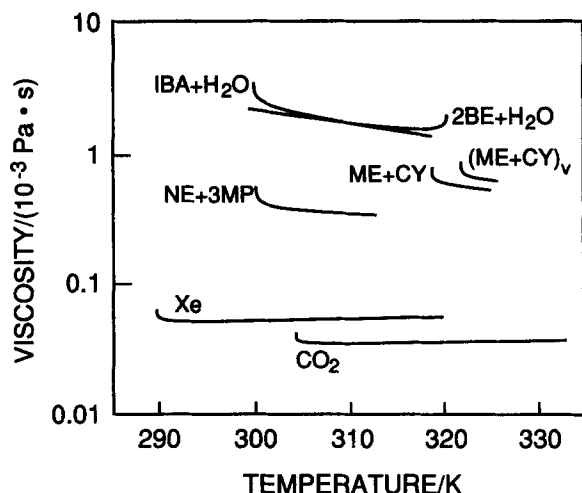


FIG. 2. The viscosities of four binary mixtures and two pure fluids near their critical points. The label (ME + CY)<sub>v</sub> denotes the methanol + cyclohexane data taken at constant volume. The other mixture data are near atmospheric pressure and the CO<sub>2</sub> and Xe data are taken on their critical isochores. The measured viscosity exponents are shown in Fig. 1. Other nonstandard abbreviations are: IBA for isobutyric acid, 2BE for 2-butoxyethanol, NE for nitroethane, and 3MP for 3-methylpentane.

The conditions of low frequency  $\omega$  and low shear rate  $\dot{\gamma}$  required for measuring the hydrodynamic viscosity

$$\omega\tau \ll 1 \quad \text{and} \quad \dot{\gamma}\tau \ll 1 \quad (4)$$

are more easily met with pure fluids than with binary liquid mixtures. At a given value of  $t$ , the relaxation time  $\tau$  of pure fluids is 10–100 times smaller than in the binary liquid mixtures we studied. As with our recent binary liquid measurements, we used a unique viscometer that operated near 1 Hz and  $\dot{\gamma} \approx 1 \text{ s}^{-1}$ . Thus the corrections to  $\omega = 0$  and  $\dot{\gamma} = 0$  were always negligible.

Near liquid–vapor critical points, the observability of the divergence of  $\eta$  is limited by gravity–induced stratification within about 10 mK of  $T_c$ . (Similar limits occur for other thermophysical properties.<sup>5</sup>) For example, although the xenon sample was only 0.7 mm high, the density inhomogeneity became 7% near  $T_c$ . The smaller height and viscosity of the liquid–vapor samples, in comparison with binary liquid mixtures, led to smaller viscous forces that were more readily obscured by ambient vibrations. The requirements of reducing temperature gradients was more stringent near liquid–vapor critical points because gradients as small as 100 mK/m in pure fluids cause strong convective flows and density inhomogeneities near  $T_c$ . Finally, in spite of our thin samples, the apparent macroscopic thermal relaxation time became as long as 1000 s in CO<sub>2</sub> and xenon, and caused hysteresis that we did not observe in any binary liquid mixture sample.

Section II outlines the theoretical context of our measurements and reviews the standard argument for a multiplicative form of the noncritical background. Section III describes the novel aspects of our apparatus and techniques. Section IV describes the samples and Sec. V describes the analysis of the data. A comparison of the present results with previous measurements appears in Sec. VI. Section VII is the conclusion.

## II. THEORETICAL EXPECTATIONS

### A. Universal critical exponent $\gamma$

Dynamic critical phenomena have been reviewed by Swinney and Henry in 1973,<sup>6</sup> by Hohenberg and Halperin in 1977,<sup>1</sup> and by Sengers in 1973<sup>7</sup> and 1985.<sup>2</sup> The universality (within classes) of the viscosity exponent is accepted by theorists.

The numerical value of the viscosity exponent is small. An early calculation using the mode-coupling theory to single-loop order gave the result<sup>8,9</sup>

$$\gamma = (8/15\pi^2)\nu \approx 0.034, \quad (5)$$

where  $\nu \approx 0.630$  is the exponent for the static correlation length. Bhattacharjee and Ferrell,<sup>4</sup> in a more recent two-loop calculation, found

$$\gamma \approx 0.032 \quad (6)$$

and they estimated that the error in this result is “of the order of 1%.” The same authors found  $\gamma = 0.034$  from a dynamic renormalization group calculation to order  $\epsilon^3$ ; however, they argued that the  $\epsilon$  expansion is less reliable for the viscosity than the mode-coupling theory.

### B. Multiplicative form for the critical viscosity

The dynamic renormalization group theory<sup>1</sup> predicts that the viscosity diverges asymptotically as  $T_c$  as in Eq. (2) or, in terms of the correlation length  $\xi$ ,

$$\eta \sim \xi^{x_\eta}, \quad (7)$$

where

$$\gamma = \nu x_\eta. \quad (8)$$

An independent theoretical approach, mode coupling, employs the idea that nonlinear couplings between relevant hydrodynamic modes can affect the values of the kinetic coefficients and thus the transport coefficients. Approximately, one has two coupled integral equations<sup>1</sup> that relate thermal conductivity and viscosity at wave vector  $k$  to each other through the  $k$ -dependent susceptibility  $\chi(k)$ . Further approximations lead to the prediction of a logarithmically diverging viscosity

$$\eta = \eta_0 [1 + (8/15\pi^2)\ln(Q_0\xi)], \quad (9)$$

where  $\eta_0$  is the noncritical fluid viscosity and  $Q_0$  is a fluid-dependent wave vector.

The dynamic renormalization group result of Eq. (7), strictly valid only in the experimentally inaccessible region where  $\eta \gg \eta_0$ , is inconsistent with Eq. (9). Ohta<sup>10</sup> pointed out that, if Eq. (9) is viewed as the first term of a power law expansion, consistency can be restored by writing, *ad hoc*,

$$\eta = \eta_0 (Q_0\xi)^{x_\eta} \quad (10)$$

or, in terms of the reduced temperature  $t$ ,

$$\eta = [\eta_0 (Q_0\xi_0)^{x_\eta}] t^{-\gamma}. \quad (11)$$

The quantity in brackets is the amplitude of the divergence and it includes the fluid-dependent quantities  $\eta_0$ ,  $Q_0$ , and  $\xi_0$ . The “multiplicative” form of Eq. (10) is not rigorous but it is useful because it specifies how to treat the noncritical

background viscosity  $\eta_0$ . The critical divergence is multiplied by the noncritical background and not added to it.

### C. Background viscosity

Although the observed increase of the viscosity is smaller near liquid–vapor critical points than near consolute points of binary liquid mixtures, the characteristic exponent is usually assumed to be the same for both cases. For both types of fluids, analysis of the experimental data is complicated by the proper separation of the noncritical viscosity  $\eta_0$  from the total viscosity. As a first step, the form of the function  $\eta_0(T)$  must be specified, using, for example, the empirical Andrade (“Arrhenius”) equation for binary liquids:

$$\eta_0(T) = Ae^{B/T}. \quad (12)$$

In the noncritical region of pure fluids, the following ansatz, though not proved valid for the critical region, is widely used for representing the viscosity of gases:<sup>11</sup>

$$\eta_0(T, \rho) = \eta_{00}(T) + \eta_{01}(\rho). \quad (13)$$

In contrast to the dense liquids used for binary liquid experiments, the temperature dependence of  $\eta_0$  is relatively weak and is apparently determined entirely by the low-density-limiting viscosity  $\eta_{00}(T)$ . Though the function  $\eta_{00}(T)$  is consistent with the predictions of kinetic theory, the density dependence  $\eta_{01}(\rho)$  is less understood at moderate densities.

### D. Crossover from critical to noncritical behavior

The use of Eq. (13) for the noncritical viscosity in the multiplicative form of Eq. (11) fails for pure fluids more than 1 K from  $T_c$ . Instead, the experimental viscosity “crosses over” to purely noncritical temperature dependence. Any “crossover” function describing this behavior must assume the asymptotic forms for the critical and noncritical temperature regions [Eqs. (11) and (13)]. Knowing the crossover function is required in order to extract the exponent  $y$  from experimental data because, in contrast to binary liquids, the region where the viscosity displays its asymptotic temperature dependence is not experimentally accessible. This is because gravitational stratification limits the measurements at reduced temperatures less than about  $t = 3 \times 10^{-5}$  and crossover from asymptotic behavior is important at reduced temperatures above about  $t = 3 \times 10^{-4}$ .

For our analysis, we used a crossover function  $H$  derived by Bhattacharjee, Ferrell, Basu, and Sengers<sup>12</sup> who included the effects of noncritical contribution to the fluctuation decay rate, as measured by a characteristic wave vector  $q_C$ , and cut off the relevant mode coupling integrals at the finite wave vector  $q_D$ . Their expression for the viscosity is

$$\eta = \eta_0 \exp[x_\eta H(q_C \xi_0, q_D \xi_0, \xi)], \quad (14)$$

with  $H$  having the required asymptotic forms

$$H = \ln(Q_0 \xi), \quad \text{close to } T_c$$

and

$$H = 0, \quad \text{far from } T_c. \quad (15)$$

Appendix A describes the function  $H$ .

Recently Olchowy and Sengers<sup>13,14</sup> improved this crossover function to allow an accurate, consistent descrip-

tion of thermal diffusivity as well as viscosity. However, unlike the earlier version, their  $H$  is not in closed form. Because the two crossover functions are equivalent for descriptions of only the viscosity,<sup>15</sup> we used the simpler form of Bhattacharjee *et al.*<sup>12</sup>

## III. APPARATUS AND TECHNIQUES

### A. Summary

The present torsion-oscillator viscometer is shown in Fig. 3. The inertial element of the oscillator was a hollow bob that contained the entire sample within a surface of revolution. The elastic element was a quartz fiber that had very low internal friction. The viscosity was derived from measurements of the decay rate, or decrement, of the torsion oscillations.

The present viscometer is an improved version of the viscometers that were used for our earlier measurements with binary liquid mixtures.<sup>3,16</sup> All these viscometers had three important accommodations for nearly critical samples. They are: (1) precise temperature control ( $< 1$  mK), which is necessary for acquiring data near  $T_c$ ; (2) low frequencies ( $\sim 1$  Hz); and (3) small oscillation amplitudes to achieve low shear rates ( $0.1\text{--}1\text{ s}^{-1}$ ). The low frequency and shear rate also ensure that viscous heating was negligible (of the order of  $10^{-12}$  W) for our  $\text{CO}_2$  and xenon samples.

### B. Differences from our earlier viscometers

#### 1. Temperature control

The thermostat for the liquid–vapor viscometer was fully controlled by software. As before, the thermostat was

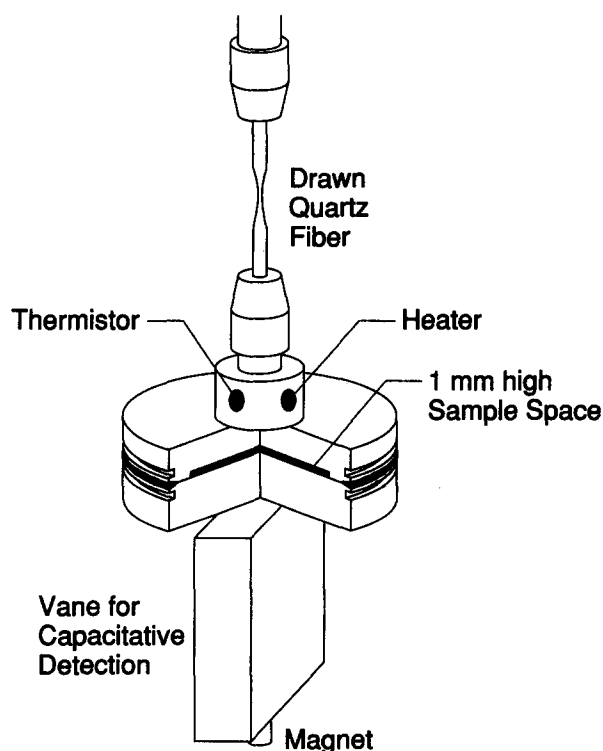


FIG. 3. The  $\text{CO}_2$  bob, shown sectioned, suspended by a drawn quartz fiber. This bob did not have an internal stiffening post and the sample height was 1 mm.

comprised of three evacuated, nested, aluminum shells thermally connected to each other primarily by radiation. The manually operated resistance bridges and analog feedback networks that had been used to control the shells' temperatures were replaced with a digital system that used a scanner, a six-digit ohmmeter, a personal computer, and computer-controlled power supplies connected to the heaters on each shell. The same instruments were used to measure the decrement. To avoid interference with the decrement measurement, the measurement of the thermistors' resistances and the updating of the proportional-derivative-integral control algorithm were implemented only once per decrement measurement, typically ten times per hour. Nevertheless, the temperature stability of the inner shell was within  $\pm 0.3$  mK. The precision of the temperature measurements was limited to  $\pm 30 \mu\text{K}$  by the resolution of the ohmmeter.

As before, the heater on the bob was not used during the viscosity measurements. Thus, the thermally isolated bob acted as a passive fourth thermostat stage with good temperature stability and small temperature gradients. The thermal equilibration time for the aluminum components of the bob was approximately 5 s and the time constant for the bob's temperature to relax, via radiation, to that of the surrounding shell was approximately  $10^4$  s. Under typical conditions close to  $T_c$ , the bob was cooling at  $0.3 \mu\text{K/s}$  and the static, environmentally induced temperature difference along the inner shell was 5 mK. These conditions implied a cooling-induced gradient on the order of  $150 \mu\text{K/m}$  and a static gradient of  $250 \mu\text{K/m}$ . The latter estimate is the upper bound expected if the bob behaved as a blackbody. The bob's low emissivity of 0.2 reduced the static gradient. We estimate that the total gradient on the bob was  $200 \mu\text{K/m}$ .

## 2. Vibration isolation

The precision of the viscosity measurements was limited by ambient vibrations. In the earlier viscometers we controlled this problem by (1) using an axial magnet attached to the bob to selectively damp out nontorsional vibrations and (2) maintaining the thermostat's vacuum with a low-vibration liquid-nitrogen-cooled sorption pump. In the present work the viscometer had a smaller sample height and the fluids studied had smaller viscosities. The viscous damping of the bob was correspondingly smaller and more easily obscured by vibrations. Thus further measures were required to deal with vibration.

Vibration isolation could not be improved with commercial isolation tables that had vertical and horizontal resonances near 1 Hz, the frequency of the torsional resonance of the viscometer. Thus, we built a special-purpose isolation table comprised of a cubical frame suspended from the ceiling by a rubber tube that acted as a torsion fiber. For this structure, the important torsional resonance occurred at 0.04 Hz. There were five other low-frequency resonances between 0.3 and 2.1 Hz (two corresponding to rotations and three corresponding to translations of the frame) that did not couple strongly to the viscometer. The frame was 0.6 m on an edge and had a 0.6 cm thick aluminum plate "floor" that supported the thermostat and sorption pump. When surrounded by a wind shield, the frame had an acceleration

noise density of  $2 \times 10^{-6} \text{ m s}^{-2}/\text{Hz}^{1/2}$  near 1 Hz in the plane of the floor.

The product of the frame's noise spectrum and the viscometer's frequency-dependent sensitivity to accelerations determined the experimental signal-to-noise ratio. We reduced the viscometer's quality factor  $Q$  to 100 by adding air to the thermostat. Then the viscometer's sensitivity to acceleration in the frequency range 0.1–10 Hz was measured with a shaker and an accelerometer. The calculated sensitivity was within a factor of 3 of that measured. These data, when combined with the measured vibration spectrum, also agreed with the observed signal-to-noise ratio of the torsion oscillator.<sup>17</sup> During the viscosity measurements the thermostat was evacuated and the  $Q$  was approximately 2000. Under these conditions the viscometer was more susceptible to vibrations below the table's lowest resonance at 0.04 Hz and the actual signal-to-noise ratio was then about half the calculated value.

## 3. Bob construction

The bobs used in the present work are constructed quite differently from those used in our earlier work with binary liquid mixtures. In common with other viscosity measurements made near liquid-vapor critical points, the samples were contained within thin, horizontal "pancake-shaped" volumes to reduce the effects of gravitational stratification and to reduce the time constant for vertical stratification.

The design of the bobs required several compromises. Thick walls were desired for high strength and stiffness; however, thin walls led to lower moments of inertia and correspondingly larger decrements. A small sample height minimized gravitational stratification and sample equilibration times near  $T_c$ ; however, a large height with a correspondingly larger sample volume would have eased the problem of loading the viscometer to the critical density. A larger height also leads to greater viscous forces and correspondingly increased immunity to ambient vibrations. Finally, the complexity of the data analysis is reduced when the viscous penetration depth  $\delta$  is a small fraction of the cell half-height  $h$ .

Figures 3 and 4 show the construction of the present bobs. The sample was contained within two aluminum parts that had been electron-beam welded together. For the xenon measurements only, the bob contained a central threaded post, which stiffened it against pressure-induced distortion. The interior surfaces of both bobs were polished with No. 600 emery paper, leaving only fine azimuthal scratches. Representative bobs were sectioned after the welding operations. The sections verified that the welding produced negligible distortions of the interior geometry.

As in our earlier work, a pin vise was attached to the upper side of each bob to clamp the quartz fiber (see Fig. 3). Electrical contacts were made to the heater, the thermistor, and the bob itself via loosely coiled, uninsulated,  $25 \mu\text{m}$  diam, gold or copper wires. A vertical vane was attached to the bottom of the bob and was used as one plate of a capacitor to detect the torsional motion of the bob. Table I lists the characteristics of the two bobs.

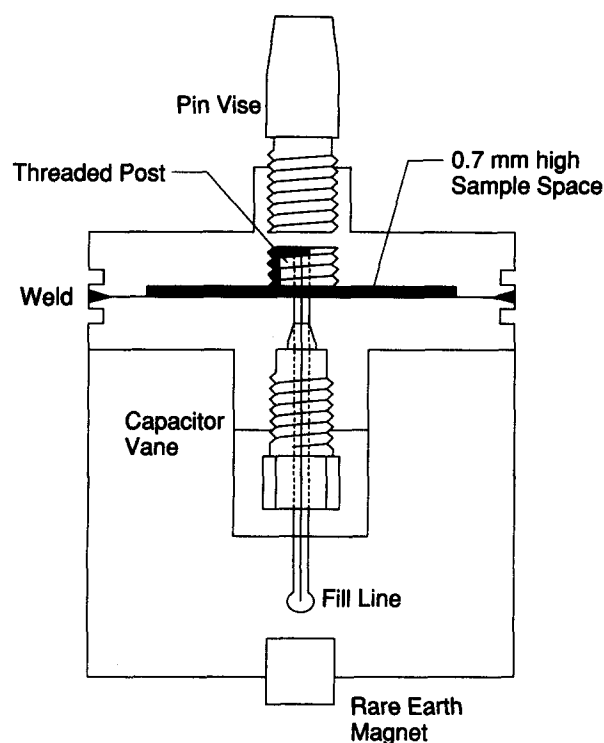


FIG. 4. Cross section of the xenon bob. The central threaded post reduced distortion of the pancake-shaped sample volume from the internal pressure while contributing negligibly to the total decrement.

#### 4. Pressure monitoring

In comparison with our earlier work, the present smaller samples of lower viscosity led to low decrements and correspondingly high sensitivity to losses of mechanical energy unrelated to the samples' viscosity. These extraneous losses, measured with the bobs and the thermostat evacuated, are denoted vacuum decrements  $D_0$ . The measurements of  $D_0$  could not be repeated after the bobs were loaded and sealed with the sample gases. In the worst case ( $\text{CO}_2$  at  $45^\circ\text{C}$ )  $D_0$  was 8% of the total decrement. The accuracy of the measurement of  $D_0$  limited the absolute accuracy of our viscosity determinations.

The vacuum decrement  $D_0$  had a linear dependence on the residual pressure in the thermostat; however, it was dominated by the pressure-independent component at the typical operating pressures of 0.03–0.06 Pa. The dependence of  $D_0$  on residual pressure was discovered only after the com-

pletion of the  $\text{CO}_2$  measurements. For the later xenon measurements we installed an ionization gauge and recorded the residual pressure in the thermostat. The xenon decrements were then corrected by the coefficient  $2.8 \times 10^{-4} \text{ Pa}^{-1}$  obtained by measuring the residual pressure dependence of the loaded bob at  $21^\circ\text{C}$ , where  $d\eta/dT \approx 0$ .

#### 5. Peltier coolers

To cool the thermostat to the critical temperature of xenon ( $T_c = 17^\circ\text{C}$ ) we attached two Peltier coolers to the outer shell of the thermostat. The hot sides of the Peltier coolers were attached to passive air-cooled aluminum "heat sinks" commonly used to cool electronic devices. Thus, waste heat was removed from the thermostat without coupling external vibrations to it. The temperature of the outer shell was regulated with a thin film heater in exactly the same way as when the shell was above room temperature.

#### C. Measurement procedure

We made decrement measurements by using a capacitance bridge to monitor the freely decaying torsion oscillations. The output of the bridge was assumed to be of the form:

$$\theta = \theta_0 \sin(\omega t) e^{-\omega t D / 2\pi}. \quad (16)$$

The initial amplitude  $\theta_0$  was typically 1 mrad and the frequency  $\omega/2\pi$  was about 1 Hz. The oscillations were monitored for 500 periods, enough for the amplitude to decrease by a factor of  $1/e$ . The decrement  $D$  was obtained by fitting an exponential to the digitized waveform peaks. Further details appear in Ref. 16.

We began measurements by rapidly heating the bob to several kelvins above  $T_c$ . This was done by dissipating 0.3 W in the heater on the bob and mixed the fluid in the bob by convection. The heater on the bob was turned off and the bob cooled freely towards the temperature of the inner shell of the thermostat. The temperatures of the shells were programmed to cool towards  $T_c$  at rates that were low enough to avoid rate dependence in the decrement measurements. During the cooling, which lasted 1 or 2 days, 10 "points" were recorded each hour. Each point included a measurement of the decrement, the temperature of the bob, and other variables such as the temperatures of the shells and the residual pressure. The decrement scatter was typically  $\pm 0.3\%$ .

Figure 5 shows the temperatures of the shells during a 2-day run. Far from  $T_c$ , the bob's cooling rate was typically  $-1 \times 10^{-4} \text{ K/s}$ , equivalent to  $-9 \text{ K/day}$ . At this rate, and for reduced temperatures  $t > 0.01$ , the temperature dependence of the viscosity and convective flows within the viscometer were both too small to cause observable hysteresis effects. This was checked by taking data while heating as well as cooling the samples.

Near  $T_c$ , much lower sweep rates were required to avoid observable hysteresis. The hysteresis was caused by the long time required for establishing the gravitationally stratified density profile and not by the viscosity's weak temperature dependence. In contrast to experimental<sup>20,21</sup> and recent theoretical<sup>22–24</sup> studies finding fast approaches to equilibrium near  $T_c$  in homogeneous fluids, we found a limiting time

TABLE I. Key characteristics of the sample cells. The volume, radius, and half-height are interior dimensions.

	$\text{CO}_2$	Xe
volume/ $\text{mm}^3$	756	525
radius $R$ /mm	15.00	15.00
half-height $h$ /mm	0.500	0.350
central post	no	yes
$I/(10^{-5} \text{ kg m}^2)$	1.389	1.393
period/s	0.973	0.681
$D_0$ , typical	$1.15 \times 10^{-4}$	$0.15 \times 10^{-4}$
$D$ , typical	$15 \times 10^{-4}$	$21 \times 10^{-4}$
$\delta$ /mm, typical	0.16	0.11

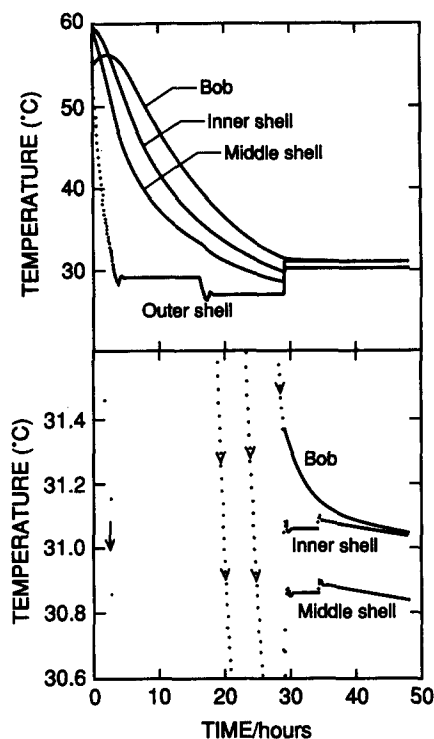


FIG. 5. A typical history of the temperatures of the thermostat shells. Although the three shells are all regulated, only the outer shell was able to cool rapidly enough to reach its programmed temperatures during the first 29 h. In the lower plot, the vertical scale is expanded to show the final temperature sweep rate of  $-1 \times 10^{-6}$  K/s ( $-1.5$  K/month).

constant of roughly  $10^3$  s, limiting us to sweep rates no greater than  $\pm 0.3 \mu\text{K/s}$  near  $T_c$ . Our slowest negative sweep rates ( $-0.3 \mu\text{K/s}$  for xenon and  $-0.05 \mu\text{K/s}$ , equivalent to  $-1.6$  K/yr, for  $\text{CO}_2$ ) gave results that were indistinguishable from the results of similarly slow positive sweeps that started in the two-phase region.

#### IV. SAMPLE PREPARATION

There are several reasons to choose  $\text{CO}_2$  and xenon for the study of the viscosity divergence. Both fluids are stable and have critical temperatures conveniently near room temperature. Xenon is of particular interest because it was chosen for a near-critical light scattering experiment to be flown on the Space Shuttle.<sup>25</sup> The present viscosity data will be used to interpret the light scattering data in the context of the mode-coupling theory of transport properties near  $T_c$ .  $\text{CO}_2$  is preferred to xenon for an Earthbound measurement because the value of  $t$  at which stratification limits the observability of the viscosity divergence is a factor of 2 smaller in  $\text{CO}_2$  than in xenon.

Both bobs were filled to within  $\pm 0.3\%$  of the critical density  $\rho_c$  using a gas burette. At  $t = 10^{-5}$ , the maximum error in the critical point enhancement of the viscosity was therefore

$$\Delta\eta(\delta\rho)/\eta < \pm 7 \times 10^{-4} \quad (17)$$

because the samples followed a near-isochore that missed  $\rho_c$  (Ref. 3).

The volume of each bob was measured as a function of

pressure by filling the bob with compressed argon and then releasing the argon into the gas burette. Then the appropriate quantity of the sample gas was condensed from the gas burette into the bob while the bob was partially submerged in a cup of liquid nitrogen. The tube leading from the burette to the bob was crimped and cut near the bob and then sealed by brazing. Auxiliary tests had established that crimping was adequate to seal the bob during the interval between the cutting and the brazing. The reproducibility of the viscosity over several months verified the integrity of the final seal.

The  $\text{CO}_2$  was asserted by the supplier<sup>26</sup> to be 99.998% pure. The xenon<sup>27</sup> was said to be 99.999% pure. The inaccuracies in loading the bobs resulted from imperfect determinations of the volumes of the bobs ( $\pm 2 \text{ mm}^3$ ) and from the uncertainties in the values for  $\rho_c$  [ $468 \pm 2 \text{ kg/m}^3$  for  $\text{CO}_2$  (Ref. 28) and  $1116 \pm 2 \text{ kg/m}^3$  for xenon<sup>29</sup>].

#### V. ANALYSIS OF DATA

Prior to considering the models for the viscosity, the decrement data were culled according to simple criteria and straightforward corrections were made. To obtain the viscosity from the corrected data, it was necessary to consider the complexity of the flow field in the viscometer. The geometry of the flow field was incorporated into a "viscometer working equation" that recognizes that the viscous penetration length

$$\delta = (2\eta/\rho\omega)^{1/2} \quad (18)$$

is not infinitesimal in comparison with the bob's radius  $R$  and half-height  $h$ . A further complication occurs in the region close to  $T_c$ , where gravity makes the sample inhomogeneous. In this region we followed the procedures of Ref. 19 and assumed that the average density was exactly  $\rho_c$  and that the density varied with height according to the "restricted cubic model" equation of state. The variation of the correlation length with height was calculated from the density profile (see Appendix B). Then the height-dependent viscosity was calculated from the correlation length via Eq. (14). Finally, the decrement was calculated approximately by integrating the appropriate function of density and viscosity over the surface bounding the fluid sample. Although the relationship between the viscosity and the decrement is complex, it was embedded in a fitting program that was used to find the best values of the parameters describing the temperature dependence of the viscosity.

In our previous work with binary liquid mixtures,  $\delta/h$  was much smaller than in the present work and stratification did not occur on the time scale of the measurements. Thus, the analysis of the earlier data was much simpler.

##### A. Data preparation

We collected several thousand data points for both  $\text{CO}_2$  and xenon. The data were culled according to several criteria. Certain blocks of data were eliminated because either the temperature was below  $T_c$ , the sweep rate was too fast, or the residual pressure in the thermostat was unacceptably high. Of the remainder, another 18% were eliminated because the standard deviation of  $D$  obtained from an exponential fit was too large. Usually this indicated that a mechanical distur-

bance occurred during the decrement measurement.

The vacuum decrement  $D_0$  was then subtracted from the culled values of  $D$ . In the case of xenon the pressure dependence of  $D_0$  was included; for  $\text{CO}_2$ , only the average pressure was used. Because  $D_0$  for  $\text{CO}_2$  was measured with a quartz fiber different from that used for the viscosity measurements, an additional correction was made to  $D_0$  reflecting the expected  $\omega^{-1}$  dependence of the pressure-dependent portion of  $D_0$ .

As a final step in preparing the decrement data for analysis, the culled data were averaged in groups of 10 points. About 4% of the data were eliminated where the groups of 10 happened to span large temperature gaps.

## B. Viscometer working equation

For a fluid-filled cylinder with a moment of inertia  $I$  oscillating at sufficiently high frequency  $\omega$  about its axis,  $\delta/R \ll 1$  and  $\delta/h \ll 1$  and the decrement can be calculated to first order in  $\delta/R$  by integrating the local dissipation per unit area<sup>30</sup> over the container's inner surface, yielding

$$D_1 - D_0 = \frac{\pi^2 R^4 [1 + 4(h/R)]}{I} \left( \frac{\eta \rho}{2\omega} \right)^{1/2}. \quad (19)$$

Equation (19) shows that  $D_1$  is a measure of  $(\eta \rho)^{1/2}$  and that only about 10% of the dissipation occurs near the vertical surface of the present viscometer; the remainder occurs near the top and bottom surfaces. For the present viscometer  $\delta/h \approx 0.3$  and the error in using Eq. (19) is as large as 10% of the actual decrement  $D$ . However, Newell and co-workers<sup>31</sup> derived an expression for  $D$  that is valid for all values of  $\delta/h$  and  $\delta/R$ :

$$[s + (D_0/2\pi)]^2 + 1 + D(s) = 0. \quad (20)$$

Five different forms for the complex function  $D(s)$  were derived. The most appropriate for the present situation ( $R \gg h > \delta$ ) is their Eq. (28a):

$$D(s) = s^2 \left( \frac{I'}{I} \right) - 8s^3 \left( \frac{I'}{I} \right) \times \sum_{j=1}^{\infty} (\mu_j s)^{-2} \left( 1 - \frac{\tanh(s_j \eta_0)}{s_j \eta_0} \right), \quad (21)$$

where

$$\begin{aligned} s &= (\omega_0/\omega) [- (D/2\pi) + i], \\ \eta_0 &= \sqrt{2}h/\delta = \text{reduced half height}, \\ \xi_0 &= \sqrt{2}R/\delta = \text{reduced radius}, \\ I' &= \pi \rho h R^4, \\ \omega_0 &= \text{oscillation frequency if } \delta = 0, \\ \mu_j &= j\text{th zero of } J_1 [J_1(\mu_j) = 0], \\ s_j^2 &= s + (\mu_j/\xi_0)^2. \end{aligned} \quad (22)$$

The sum in Eq. (21) converges very slowly; hundreds of complex terms are required to obtain the necessary accuracy. In fact, for sufficiently small  $\delta$ , double precision roundoff errors caused failure of Newton's method when solving Eq. (20). Grouvel and Kestin<sup>32</sup> obtained a simple analytic working equation from Eq. (20) and Eq. (21) which, to  $O(\delta/R)^2$ , is

$$\begin{aligned} D_2 - D_0 &= \left( \frac{\pi I'}{2I} \right) \left( \frac{\delta/\sqrt{2}}{R} \right) \left[ \left( 4 + \frac{R}{h} \right) \right. \\ &\quad \left. - \left( \frac{\delta/\sqrt{2}}{R} \right) \left[ \left( 6 + \frac{6R}{\pi h} \right) + \left( \frac{I'}{I} \right) \left( 4 + \frac{R}{h} \right)^2 \right] \right]. \end{aligned} \quad (23)$$

To within 0.3%, Eq. (23) agrees with the exact result derived from the numerical solution of Eqs. (20) and (21) in the ranges of  $\delta/R$  and  $\delta/h$  appropriate to the  $\text{CO}_2$  and xenon samples.

## C. Accounting for stratification

Here we estimate the effects of stratification by combining the vertical profiles of the density and the viscosity with the  $O(\delta/R)$  and  $O(\delta/R)^2$  formulas for the decrement. We have not done additional analysis of the flow field. Instead, we argue that this combination is a reasonable approximation on physical grounds.

As noted above, 90% of the dissipation occurred within  $\delta$  of the top and bottom surfaces of the viscometer. At these locations, the values of  $\eta - \eta_c$  and  $\rho - \rho_c$  are largest; however, the changes of  $\eta$  and  $\rho$  in a height  $\delta$  are small compared with  $\eta - \eta_c$  and  $\rho - \rho_c$ . We ignored these changes and used the  $O(\delta/R)^2$  formula Eq. (23) to compute the decrements

$$D_z^\pm \equiv D_2[\eta(\pm h), \rho(\pm h)] \quad (24)$$

expected if the bob were filled homogeneously with fluid having the viscosity and density found at the bottom ( $-h$ ) and top ( $+h$ ) of the bob. The variation of  $\eta$  and  $\rho$  with height along the side wall was then accounted for by the integrals

$$\begin{aligned} D_1^\pm &= \int_{-h}^{+h} (D_1'[\eta(z), \rho(z)] \\ &\quad - D_1'[\eta(\pm h), \rho(\pm h)]) dz. \end{aligned} \quad (25)$$

Here,

$$D_1'(z) \equiv \frac{1}{2} \frac{\partial D_1}{\partial h} \quad (26)$$

is the  $O(\delta/R)$  formula for the decrement per unit height for the cylinder's side wall. The integrals thus measure the difference  $\sqrt{\eta(z)\rho(z)} - \sqrt{\eta(\pm h)\rho(\pm h)}$  on the side wall. Finally, the total decrement was calculated from the average

$$D = (D_1^+ + D_1^- + D_2^+ + D_2^-)/2. \quad (27)$$

We estimated the difference between our approximate algorithm and the unknown exact solution for  $D$  to be a few tenths of a percent at most. This is because (1) the density deviation  $[\rho(h) - \rho_c]/\rho_c$  was only a few percent and (2) to first order in  $[\rho(h) - \rho_c]/\rho_c$ , the terms  $\sqrt{\eta[\rho(\pm h)]\rho(\pm h)}$  for the top and bottom walls average to  $\sqrt{\eta[\rho(0)]\rho(0)}$  if the rather small increase in  $\eta$  near the critical point is ignored.

## D. Further approximations

We made several additional approximations in the analysis that were checked with the  $O(\delta/R)$  formula of Eq. (19). First, we ignored thermal expansion of the bob, which

changed its radius  $R$  and moment of inertia  $I$ . Second, we assumed the oscillator's period remained constant. Third, we ignored the effect of the central post in the xenon cell. Fourth, we ignored the pressure-induced expansion of the sample volume at temperatures well above  $T_c$ . The worst-case errors caused by these approximations are listed in Table II.

Within 3 K of  $T_c$  the maximum error in these approximations was less than 0.3%. The accuracy of the viscosity measurements was not affected by these approximations because their effects are smaller than the uncertainty in the viscometer's dimensions (Table I) and the vacuum decrement  $D_0$  (Table IV).

### E. Background viscosity

The noncritical background viscosity  $\eta_0$  was represented by the ansatz of Eq. (13), repeated here:

$$\eta_0(T, \rho) = \eta_{00}(T) + \eta_{01}(\rho). \quad (28)$$

The correlation developed by Kestin and co-workers<sup>33,34</sup> was used to determine  $\eta_{00}$ :

$$\eta_{00} = \frac{5(mk_B T/\pi)^{1/2}}{16 \sigma^2 \Omega}. \quad (29)$$

Here  $m$  is the molecular mass,  $k_B$  is the Boltzmann constant, and the parameter  $\sigma$  and the empirical function  $\Omega$ , related to the collision integral, were fit to the data. We used the description obtained by Iwasaki and Takahashi<sup>35</sup> for  $\eta_{01}$  ( $\text{CO}_2$ ). To describe  $\eta_{01}$  (xenon) we combined the correlating function of Jossi, Stiel, and Thodos<sup>36</sup> with the data of Reynes and Thodos.<sup>37</sup> Appendix C give the numerical details of the background viscosity descriptions.

### F. Crossover function

The total viscosity was represented by Eq. (14), which is a product of the noncritical viscosity  $\eta_0$  and an exponential containing a universal crossover function  $H$  that depends on the two nonuniversal parameters  $q_c \xi_0$  and  $q_D \xi_0$ . Recently, Olchowy and Sengers<sup>13,14</sup> used mode coupling theory to derive a complicated expression for the crossover function  $H$  as part of a consistent description of both the viscosity and thermal conductivity of pure fluids. However, an earlier, much simpler expression for  $H$  (Ref. 12), though not consistent with the thermal conductivity, gives equivalent results for the viscosity.<sup>15</sup> We used this older formulation, described in Appendix A. The fluid-dependent parameters in  $H$  were the products of the wave vectors  $q_c$  and  $q_D$  with the correlation length amplitude  $\xi_0$ . Data determining  $q_c$  and  $\xi_0$  were available for both  $\text{CO}_2$  and xenon. The careful thermal conductivity measurements required to determine  $q_D$  were not avail-

able for xenon. Thus,  $q_D$  was treated as an adjustable parameter in fitting the xenon decrement data. For the  $\text{CO}_2$  decrement data, fits were made fixing  $q_D$  to the value determined from thermal conductivity and other fits were made adjusting  $q_D$ .

### G. Thermostat outgassing

As mentioned in the apparatus section, the residual pressure was not measured for the  $\text{CO}_2$  runs and its effect on the background "vacuum" decrement was assumed to be independent of temperature. We re-examined this assumption after finding that the decrements were anomalously large at temperatures above 40 °C (see Fig. 6). The vacuum decrement data acquired after installing the ionization gauge in the thermostat indicated that extra outgassing could have been sufficiently great to have caused the anomalous decrements. We were able to reconstruct an approximation to the pressure history during the affected runs; however, the reconstruction could not be used to correct the data reliably because the pressure depended sensitively upon the history of both the thermostat and sorption pump. Therefore, two alternatives were used to deal with the affected data. First, we replaced the constant vacuum decrement with a linear function of the temperature:

$$D_0 \rightarrow D_0 + (3 \times 10^{-4})t, \quad (30)$$

that approximates the effects of outgassing. Second, we fitted only to the lowest-temperature data ( $t < 10^{-2}$ ) without any pressure correction. Both alternatives affected only the data far from  $T_c$  and, as expected, they yielded similar results for the exponent  $y$ .

### H. Nonlinear least-squares fit to $D$

We fit our model for the decrement  $D$  to the data between the reduced temperatures

$$t_{\min} < t < t_{\max}. \quad (31)$$

For the  $\text{CO}_2$  data, as mentioned above, both  $t_{\max} = 0.1$  and  $t_{\max} = 0.01$  were used. For the xenon data,  $t_{\max} = 0.1$  was used. For both fluids,  $t_{\min}$  was determined by eliminating all averaged data below an initial estimate of  $T_c$ . The fitted value of  $T_c$  was always within 2 mK of  $t_{\min}$ .

Figures 6 and 7 show the decrement data and fitted descriptions for  $\text{CO}_2$  and xenon. The four free parameters in our model were  $T_c$ ,  $y$ ,  $q_D$ , and  $D_{01}$ , where  $D_{01}$  was the part of  $D_0$  not already accounted for by measurements of the vacuum decrement and the thermostat pressure, namely,

$$D_{01} \equiv D_0(\text{fit}) - D_0(\text{expected}). \quad (32)$$

In practice we fitted the quantity  $\ln(q_D \xi_0)$  to avoid unphysical negative values for  $q_D$ .

For the  $\text{CO}_2$  data we either made the plausible though *ad hoc* correction of Eq. (30) or eliminated data at  $t > 0.01$ . We also tried fixing  $q_D^{-1}$  at the value of 0.23 nm determined by analysis of thermal conductivity data.<sup>13,14</sup> Table III summarizes the results of the various fits. The narrow range spanned by the various values of  $y$  is striking.

Table IV in Appendix D contains numerical values of the viscosities of  $\text{CO}_2$  and xenon calculated from the background viscosity functions described in Appendix C, the

TABLE II. Approximations in analysis of decrement data.

Approximation	$\Delta D/D \times 10^3$
Zero thermal expansion ( $T_c + 30$ K)	+ 1
Constant period	$\pm 1$
Neglect central post in xenon cell	- 1
Neglect pressure expansion ( $\text{CO}_2$ at $T_c + 30$ K)	- 8

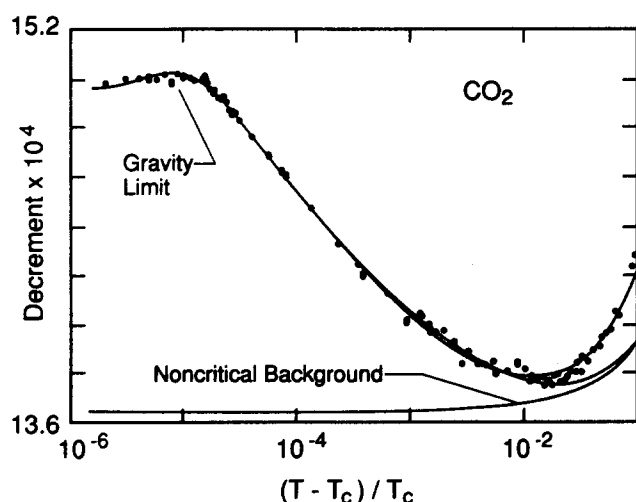


FIG. 6. The decrement of the torsion oscillator filled with  $\text{CO}_2$  as a function of the reduced temperature. Except in the gravity-limited region near  $T_c$ , the decrement is approximately proportional to  $\sqrt{\eta}$ . By means of Eq. (27) two curves were fit to the data: The upper curve accounts for thermostat outgassing with an *ad hoc* decrement proportional to the reduced temperature (parameters from second line of Table III). The middle curve was fit to data only at reduced temperatures less than  $10^{-2}$  (first line of Table III). Near  $T_c$ , stratification limited the decrement to  $<15.0 \times 10^{-4}$ .

crossover function of Appendix A, and the fit parameters in the first and last lines of Table III.

## VI. COMPARISON WITH OTHER RESULTS

This section first discusses the absolute accuracy of our viscometer both as a check for unknown systematic effects and also because errors in the absolute viscosity contribute, though weakly, to errors in the viscosity exponent. For example, an error  $\Delta\eta_0/\eta$  in the background viscosity leads to an error

$$\Delta y/y = (\Delta\eta_0/\eta) \quad (33)$$

in the viscosity exponent. The present results for the viscosity exponent are then compared with previous results.

The absolute accuracy of the present viscosity measurements is limited by our imperfect knowledge of the properties of the bobs and their samples. We used the  $O(\delta/R)$  expression for  $D$ , Eq. (19), to estimate the inaccuracy of the derived viscosity. We assumed the various contributing errors to be normally distributed and uncorrelated and thus added them in quadrature to obtain the total expected error  $\Delta\eta/\eta$ . The first part of Table IV lists the various contributing errors. The second part lists the total errors of the present results and those of Refs. 35 and 37 from which we obtained the background viscosities  $\eta_0$ . (We estimated the error of Ref. 37 from the stated uncertainty in the capillary radius.) The bottom line gives the discrepancy between the present results and those of Refs. 35 and 37. (This was done by using the part  $D_{01}$  of the decrement not explicitly accounted for by the model.) For both  $\text{CO}_2$  and xenon these discrepancies are consistent with the total combined errors.

During the last 15 years, viscosity measurements on isotherms showed increases of 10%–20% near the critical points of  $\text{CO}_2$  (Ref. 35), ethane,<sup>35</sup> water,<sup>38</sup> nitrogen,<sup>39</sup> and

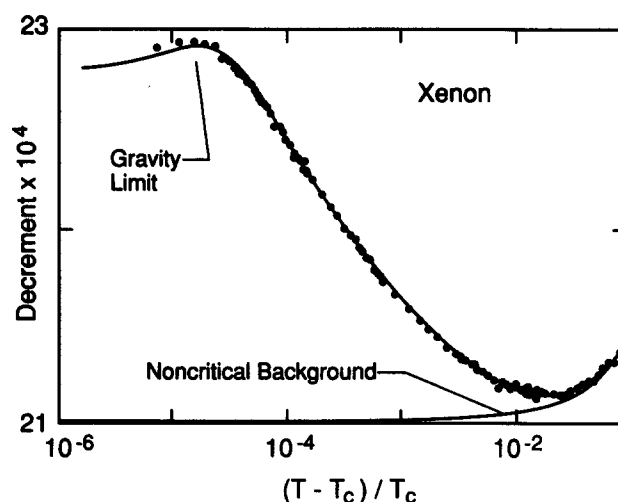


FIG. 7. The decrement of the torsion oscillator filled with xenon as a function of the reduced temperature. The curve is determined by Eq. (27) and the parameters from the last line of Table III.

ethylene.<sup>40</sup> These data are too sparse and too far from the critical point to determine  $y$  accurately.

There have been few isochoric measurements of viscosity near liquid–vapor critical points, although they are more useful for determining  $y$ . The most recent measurements were made by Agosta *et al.* with  $^3\text{He}$  and  $^4\text{He}$  in a pancake-shaped, 158 Hz torsion oscillator.<sup>19</sup> They used the crossover function generalized by Olchowy and Sengers<sup>13,14</sup> to handle thermal conductivity as well as viscosity and found that their data are better represented with  $y \equiv 0.034$  than with  $y \equiv 0.040$ . Another recent analysis of their data<sup>13</sup> found that the larger value of  $y \equiv 0.038$  is more consistent with thermal conductivity data than  $y \equiv 0.034$ .

Using the present, simpler form of the crossover function we have reanalyzed the  $^3\text{He}$  data of Agosta *et al.* which they refer to as  $\tilde{\eta}/\tilde{\eta}$  though without attempting a re-separation of their background  $\tilde{\eta}$  from the total effective viscosity  $\tilde{\eta}$ . Improvements to their analysis included using the asymptotically correct universal parameters and exponents found in Ref. 5 and allowing simultaneous fits of the viscosity exponent  $y$ , the wave vector  $q_c$ , and the critical temperature  $T_c$ . We found  $y = 0.036 \pm 0.002$  where the uncertainty reflects possible errors due to  $\rho \neq \rho_c$ . The effects of shear, frequency, or the length ratio  $\xi/\delta$  could not explain the discrepancy between this result and the present exponents for  $\text{CO}_2$  and xenon.

Bruschi and Torzo<sup>18</sup> used a disk-shaped rotor to shear  $\text{CO}_2$  contained within a flat cell. They described their data as simply the product of a critical power-law divergence and a constant noncritical background and obtained an exponent of  $y = 0.036 \pm 0.002$ . An analysis of their data with a modern crossover function has been attempted by others and resulted in the claim that these data are inconsistent with crossover theory.<sup>13,19</sup>

Strumpf *et al.* used a 40 kHz torsion crystal to measure the viscosities of xenon and ethane near their critical points and deduced the exponent values 0.031 and 0.034, respectively;<sup>41</sup> however, these data cannot be corrected to zero

TABLE III. Results of four fits to the data including  $1\sigma$  error estimates.

Fluid	Eq. (30)	$t_{\max}$	$y \times 1000$	$\ln(q_d \xi_0)$	$\Delta T_c / \text{mK}$	$D_{01} \times 10^5$
CO <sub>2</sub>	no	0.01	$40.79 \pm 0.68$	$-1.99 \pm 2.59$	0.12	$+1.44 \pm 0.16$
CO <sub>2</sub>	yes	0.1	$41.66 \pm 0.29$	$-1.65 \pm 0.15$	0.15	$+1.45 \pm 0.09$
CO <sub>2</sub>	yes	0.1	$40.96 \pm 0.21$	$-0.43 \text{ fixed}$	0.18	$+0.96 \pm 0.04$
Xe	no	0.1	$40.50 \pm 0.16$	$-1.75 \pm 0.05$	0.23	$-3.12 \pm 0.05$

frequency reliably.

Hoogland and Trappeniers used a constant-volume horizontal capillary viscometer to measure SF<sub>6</sub> near its critical points.<sup>42</sup> Their preliminary analysis found the rather high value of  $y = 0.050$ ; restricting the data to the range  $10^{-4} < t < 10^{-3}$  reduced  $y$  to 0.043. However, recent work from the same laboratory found the presence of large systematic errors due to the enormous compressibility near the critical point.<sup>43</sup>

To summarize, previous determinations of  $y$  in pure fluids are generally lower than our own values. Except for the helium results of Agosta *et al.* and the CO<sub>2</sub> results of Bruschi and Torzo, this can be expected because systematic errors due to shear, frequency, inaccurate sample loading, or inadequate temperature control limit the maximum value of the correlation length attained within the viscometer and thus the observable increase of the viscosity near the critical point. In contrast to Ref. 18 our CO<sub>2</sub> data are consistent with crossover theory. However, we cannot explain the lower exponents by Agosta *et al.* for <sup>3</sup>He and <sup>4</sup>He.

Our recent measurements on binary liquid mixtures were in part motivated by the wide range of reported values for the viscosity exponent  $y$ . Values from 0.032 to 0.042 were listed in the recent review of Ref. 2, for example. Much of this variation has been later eliminated by accounting for shear effects either by limiting the temperature range of the data, as was done by Calmettes,<sup>44</sup> or by applying corrections to the data, as was done by Nieuwoudt and Sengers.<sup>45</sup> In particular, Nieuwoudt and Sengers found that viscosity exponents derived from the shear-corrected data of six out of seven binary mixtures fell in the range

$$0.037 < y < 0.043, \quad (34)$$

with triethylamine + water being the single exception at  $y = 0.034$ . Our own measurements have been the only ones not requiring shear corrections close to  $T_c$ . They yielded

TABLE IV. Contributions to errors in the absolute viscosity and comparison with other determinations of  $\eta_0$ .

Error source	CO <sub>2</sub>	Xe
$D_0$	$\pm 1.3\%$	$\pm 0.4\%$
$R$	0.3	0.3
$h$	0.6	0.6
$I$	0.3	0.1
$\omega$	0.2	0.2
$\rho$	0.2	0.2
$\Delta\eta/\eta$ (NIST) (quadrature sum)	$+1.5\%$	$\pm 0.8\%$
$\Delta\eta/\eta$ (other)	$\pm 0.3\%$ (Ref. 35)	$\pm 8.1\%$ (Ref. 27)
$[\eta_0(\text{NIST}) - \eta_0(\text{other})]/\eta_0$	$+2.0\%$ (Ref. 35)	$-2.9\%$ (Ref. 37)

exponents in the slightly higher and narrower range of

$$0.040 < y < 0.044. \quad (35)$$

## VII. CONCLUSIONS

### A. Viscosity exponent $y$

The present liquid-vapor results for the viscosity exponent  $y$ , listed in Table III, agree much better with our previous liquid results<sup>3</sup> than with the current theoretical value. Figure 1 shows this by plotting  $y$  versus the noncritical slope parameter  $B$ , defined by

$$B \equiv \left[ \left( \frac{T_c}{\eta_0} \right) \left( \frac{d\eta_0}{dT} \right) \right]_{T_c}. \quad (36)$$

Any apparent dependence of  $y$  on  $B$  presumably reflects systematic errors in the measurements or incorrect features in the models used to describe the data. For example, we did not use a crossover function for the binary liquids.

### B. Importance of crossover

Figure 8 illustrates the necessity of a crossover model by extrapolating our results in reduced gravity. In  $10^{-4}$  g the asymptotic region reveals itself as a straight line of slope approximately  $y/2$ . However, extending this line by hand downwards shows the eye that, in 1 g, the asymptotic region is never reached! Correct models that include the effects of gravity and crossover are necessary for determining the viscosity exponent  $y$ .

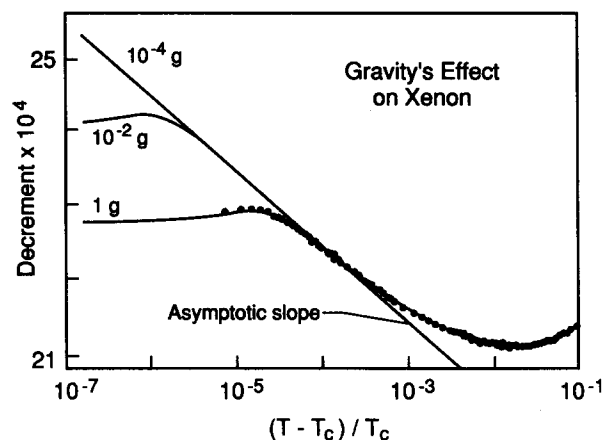


FIG. 8. The decrement expected if the xenon experiment were repeated in environments where the gravitational acceleration was  $10^{-2}$  and  $10^{-4}$  of that on the surface of the earth. To first order, the asymptotic slope is  $y/2$ . Because the asymptotic region is unavailable in 1 g, determination of the viscosity exponent  $y$  strongly depends on the theory of crossover between the noncritical and critical regions.

Because the best available crossover function comes from the same mode coupling theory which predicts too low a value for  $y$ , one might object that experimental exponents determined in this context are no more valid than the theoretical exponent. However, Bhattacharjee has argued that this is not true because the crossover function is less sensitive to details of the theory than the calculation of the exponent.<sup>46</sup>

### C. Implications for low gravity experiments

The University of Maryland experiment "Zeno"<sup>25</sup> is scheduled for Space Shuttle flight USML-1 and will obtain the critical part of the thermal diffusivity  $D_c$  from measurements of the autocorrelation of light scattered from xenon within 100  $\mu$ K of  $T_c$ . These measurements can be related to the viscosity  $\eta$  and its exponent  $y$  by<sup>47</sup>

$$D_c = (Rk_B T / 6\pi\eta\xi) \Omega(x) (1 + b^2 x^2)^{y/2\nu}, \quad (37)$$

where  $R$  and  $b$  are universal dimensionless constants,  $k_B$  is the Boltzmann constant,  $\xi$  is the correlation length with exponent  $\nu$ ,  $x \equiv q\xi$  is the scaled light scattering wave vector, and  $\Omega(x)$  is the Kawasaki function. To estimate the influence of the viscosity on  $D_c$  we used the  $x \gg 1$  limit to reduce Eq. (37) to

$$D_c = (Rk_B T q / 16\eta_0) (bq/Q_0)^{y/\nu}, \quad (38)$$

where  $Q_0$  is the fluid-dependent quantity defined in Appendix A. The error in determining  $D_c$  independently from the light scattering measurements is thus influenced by the viscosity parameters  $\eta_0$ ,  $Q_0$ , and  $y$ .

In Table V we have listed the uncertainties in these parameters for xenon and the resulting errors in  $D_c$  derived using Eq. (38). The uncertainty of  $\eta_0$  assumed the absolute accuracy of our viscometer was limited only by the measurement errors listed in Table IV. The uncertainty in  $Q_0$  came from the uncertainties in  $q_D$  (negligible) and  $q_c$ . The uncertainty in  $q_c$  in turn came from crude estimates of the parameter errors in the definition of  $q_c$  (see Appendix A). The uncertainty in  $y$  is the conservative spread formed by the union of all the CO<sub>2</sub> and xenon error bars in Table III. The error in  $D_c$  is therefore not limited by the error in the viscosity exponent  $y$  but by the errors in the noncritical parameters  $\eta_0$  and  $q_c$ .

The uncertainties in Table V are estimates due to systematic errors and are more important than the viscosity uncertainty determined solely by the precision of the decrement fits. This was verified by using the fit parameters of Table III to extrapolate the viscosity to smaller reduced temperatures allowed by a low gravity experiment. At  $t = 3 \times 10^{-7}$ , the minimum and maximum viscosities, as determined by trying all parameter sets within the  $1\sigma$  error ellipsoid centered on the best fit parameters, varied from the

value obtained by an extrapolation with the best fit parameters by only  $\pm 0.1\%$ .

### D. The need for improved calculation of $y$

We conclude from our study of four binary liquid mixtures and two pure fluids that the viscosity exponent  $y$  has a universal value:

$$y = 0.042 \pm 0.002. \quad (39)$$

This value differs from theory by 30% and has an error of only 5%. In contrast, experimental measurements<sup>48</sup> and renormalization group calculations<sup>49</sup> of the static correlation exponent  $\nu$  have converged to within 2% agreement.<sup>48</sup> We urge that a theoretical effort, commensurate in scale with the present experimental effort, be made in an attempt to resolve the discrepancy.

### ACKNOWLEDGMENTS

The authors have benefited from the critical comments and stimulation of J. K. Bhattacharjee, R. A. Ferrell, R. W. Gammon, G. Morrison, H. Meyer, J. M. H. Levelt Sengers, G. A. Olchowy, J. V. Sengers, and R. A. Wilkinson. We are grateful to U. Narger and D. A. Balzarini for providing their recent results on the critical density of xenon and to G. A. Olchowy for providing a floppy disc with the <sup>3</sup>He viscosity data of Agosta *et al.* This work has been supported in part by NASA under contract C-86129D.

### APPENDIX A: CROSSOVER FUNCTION

The viscosity crossover function  $H$  of Bhattacharjee, Ferrell, Basu, and Sengers<sup>12</sup> is

$$\begin{aligned} H = & \frac{1}{2} \sin(3\psi_D) - (1/4q_c\xi) \sin(2\psi_D) \\ & + (1/q_c\xi)^2 [1 - \frac{1}{4}(q_c\xi)^2] \sin(\psi_D) \\ & - (1/q_c\xi)^3 [1 - \frac{1}{2}(q_c\xi)^2] \psi_D \\ & - |(q_c\xi)^2 - 1|^{3/2} L(w). \end{aligned} \quad (A1)$$

The previously undefined quantities in Eq. (A1) are

$$\begin{aligned} \psi_D = & \cos^{-1} \{ [1 + (q_D\xi)^2]^{-1/2} \}, \\ L(w) = & \ln[(1+w)/(1-w)], \quad q_c\xi > 1, \\ L(w) = & 2 \tan^{-1} |w|, \quad q_c\xi < 1, \\ w = & |(q_c\xi - 1)/(q_c\xi + 1)|^{1/2} \tan(\psi_D/2). \end{aligned} \quad (A2)$$

Close to  $T_c$ , the correlation length  $\xi$  is large compared to the inverse wave vectors  $q_c^{-1}$  and  $q_D^{-1}$  and the crossover expression for the viscosity,

$$\eta = \eta_0 \exp[x_\eta H(q_c\xi_0, q_D\xi_0, \xi)], \quad (A3)$$

reduces to the simple multiplicative form

$$\eta = \eta_0 (Q_0\xi)^{x_\eta}, \quad (A4)$$

where  $\eta_0$  is background noncritical viscosity and

$$\frac{1}{Q_0} \equiv \left( \frac{e^{4/3}}{2} \right) \left( \frac{1}{q_c} + \frac{1}{q_D} \right). \quad (A5)$$

The wave vector  $q_D$  is the upper limit of the mode coupling integral for the viscosity enhancement due to critical fluctuations.

TABLE V. Errors in determining the critical diffusivity from viscosity parameters.

Parameter	Parameter uncertainty	$\Delta D_c / D_c$
$\eta_0$	1.0%	1.0%
$Q_0$	15	1
$y$	2.2	0.7

The wave vector  $q_c$  measures the relative influences of the bare and critical thermal conductivities on the fluctuation decay rate and, at the critical point, is given by

$$q_c \equiv \frac{k_B P_c \Gamma^+}{16\eta_0 \lambda_0 \xi_0^2} \left[ \frac{T_c}{P_c} \left( \frac{\partial P}{\partial T} \right)_{\rho_c} \right]^2. \quad (\text{A6})$$

Here  $P_c$ ,  $T_c$ , and  $\rho_c$  are the critical pressure, temperature, and density,  $\eta_0$  and  $\lambda_0$  are the noncritical viscosity and thermal conductivity,  $\xi_0$  is the correlation length amplitude, and  $\Gamma^+$  is the normalized amplitude of the compressibility. All of the values listed in Table VI were taken from the compilations in Ref. 49 except where noted otherwise.

The resulting values for  $q_c \xi_0$  are 0.031 for  $\text{CO}_2$  and 0.058 for xenon. The fitted values for  $q_D \xi_0$  and  $\gamma$  are in Table III.

## APPENDIX B: SAMPLE STRATIFICATION

In Ref. 5, Moldover *et al.* made use of the “restricted cubic model” expressions<sup>53</sup> for the reduced temperature  $t$ , density  $\Delta\rho$ , and chemical potential  $\Delta\mu$  and connected the reduced chemical potential to the height  $\Delta z$  in the cell by

$$\Delta z = -H_0 \Delta\mu, \quad (\text{B1})$$

where

$$H_0 \equiv P_c / \rho_c g_0, \quad (\text{B2})$$

defines a gravity scale height in the Earth’s gravity  $g_0$  in terms of the fluid’s critical pressure  $P_c$  and density  $\rho_c$ . The reduced temperature, height, and density are then expressed in terms of the parametric variables  $r$  and  $\theta$ :

$$t = r(1 - b^2 \theta^2), \quad (\text{B3})$$

$$\Delta z = -H_0 a r^{\beta\theta} (1 - \theta^2), \quad (\text{B4})$$

$$\Delta\rho = r^{\beta} k \theta (1 + c \theta^2). \quad (\text{B5})$$

The dimensionless quantities  $a$  and  $k$  are fluid-dependent but  $b$  and  $c$  are universal constants.

We used Newton’s method to solve Eqs. (B3) and (B4) for  $r$  and  $\theta$  when given  $t$  and  $\Delta z$ , then used Eq. (B5) to calculate the height-dependent density. We calculated the height-dependent viscosity by using the height-dependent correlation length,

$$\xi = \xi_0 r^{-\nu} (1 + 0.16 \theta^2), \quad (\text{B6})$$

in the crossover function  $H(\xi)$ .

The height  $\Delta z$  in the above equations specifies a location relative to the level where  $\rho = \rho_c$ . The simplifying assumption

TABLE VII. Parameters for  $\eta_{00}(T)$ .

Parameter	$\text{CO}_2$	Xe
$m/10^{-24} \text{ kg}$	7.31	1.8
$\sigma/\text{nm}$	0.3703	0.3848
$\epsilon/\text{K}$	266.13	285.27
$\Omega_0$	+0.46461	+0.45667
$\Omega_1$	−0.56612	−0.53955
$\Omega_2$	+0.19565	+0.18265
$\Omega_3$	−0.0303	−0.03629
$\Omega_4$	0	+0.00241

tion that this level occurred in the middle of the bob caused negligible error because we loaded our bobs to within 0.3% of  $\rho_c$ . However, we considered the more general case when examining the  $^3\text{He}$  data from Agosta *et al.*<sup>16</sup> at various densities. The  $\rho = \rho_c$  reference level, located a distance  $z_1$  below the sample midline, is then determined by the average density  $\bar{\rho}$ , namely,

$$\bar{\rho} = \frac{1}{2h} \int_{-h+z_1}^{+h+z_1} \rho(\Delta z) d(\Delta z), \quad (\text{B7})$$

where  $h$  is half the height of the sample. As in Ref. 19, we used a bisection root finder to determine the height  $z_1$  from Eq. (B7).

## APPENDIX C: BACKGROUND VISCOSITY

Section V E tells how the background viscosity was described by

$$\eta_0 = \eta_{00}(T) + \eta_{01}(\rho), \quad (\text{C1})$$

where

$$\eta_{00} = 5(mk_B T/\pi)^{1/2}/16\sigma^2\Omega \quad (\text{C2})$$

contains the empirical function  $\Omega(T)$ . This function, closely related to the collision integral, is described by

$$\ln[\Omega(T)] = \sum_{i=0}^4 \Omega_i \left( \ln \frac{T}{\epsilon} \right)^i. \quad (\text{C3})$$

Table VII contains the parameters for  $\eta_{00}(\text{CO}_2)$  (Ref. 33) and  $\eta_{00}(\text{Xe})$  (Ref. 34). The density-dependent description in Ref. 35 for  $\text{CO}_2$  is

$$\eta_{01}(\text{CO}_2) = \sum_{i=1}^4 a_i \rho^i, \quad (\text{C4})$$

and, from Refs. 36 and 37, for xenon is

$$\eta_{01}(\text{Xe}) = \left\{ \left[ \sum_{i=0}^4 a_i \left( \frac{\rho}{\rho_c} \right)^i \right]^4 - 10^{-4} \right\} (10^{-3}/0.01505). \quad (\text{C5})$$

TABLE VI. Parameters for evaluating Eq. (A6).

Parameter	$\text{CO}_2$	Xe
$T_c$	304.1 K	289.7 K
$P_c$	7.37 MPa	5.84 MPa
$\rho_c$	468 kg/m <sup>3</sup>	1110 kg/m <sup>3</sup>
$\xi_0$	0.15 nm	0.19 nm
$\eta_0$	$3.4 \times 10^{-5} \text{ Pa s}$ (Ref. 35)	$5.3 \times 10^{-5} \text{ Pa s}$ (Ref. 37)
$\lambda_0$	0.048 W/K m (Ref. 50)	0.017 W/K m (Ref. 51)
$\Gamma^+$	0.052	0.058
$\left( \frac{T_c}{P_c} \right) \left( \frac{\partial P}{\partial T} \right)_{\rho_c}$	6.0	5.8 (Ref. 52)

TABLE VIII. Parameters for  $\eta_{01}(\rho)$ . All units are mks.

Parameter	$\text{CO}_2$	Xe
$a_0$	0	+0.10230
$a_1$	$+7.426595 \times 10^{-9}$	+0.023364
$a_2$	$+5.872209 \times 10^{-11}$	+0.058533
$a_3$	$+1.768551 \times 10^{-14}$	−0.040758
$a_4$	$+1.149060 \times 10^{-18}$	+0.0093324

TABLE IX. Viscosity in  $\mu\text{Pa s}$  of  $\text{CO}_2$  and xenon on the critical isochore.

$\log_{10}(t)$	$\eta(\text{CO}_2)$	$\eta(\text{Xe})$
-7.00	49.78	76.84
-6.75	48.62	75.08
-6.50	47.50	73.35
-6.25	46.40	71.67
-6.00	45.33	70.02
-5.75	44.29	68.42
-5.50	43.28	66.86
-5.25	42.29	65.35
-5.00	41.33	63.88
-4.75	40.41	62.45
-4.50	39.52	61.08
-4.25	38.67	59.76
-4.00	37.87	58.50
-3.75	37.11	57.31
-3.50	36.40	56.21
-3.25	35.76	55.19
-3.00	35.19	54.27
-2.75	34.70	53.47
-2.50	34.30	52.80
-2.25	34.00	52.27
-2.00	33.81	51.92
-1.75	33.76	51.77
-1.50	33.88	51.87
-1.25	34.22	52.32
-1.00	34.86	53.24

Table VIII contains the parameters  $a_i$  which yield  $\eta_{01}$  in units of  $\text{Pa s}$ .

#### APPENDIX D: VISCOSITY VALUES

Table IX lists viscosity values for  $\text{CO}_2$  and xenon as a function of reduced temperature  $t$ . We assumed  $T_c(\text{CO}_2) = 304.13 \text{ K}$  and  $T_c(\text{Xe}) = 289.72 \text{ K}$ . The  $\text{CO}_2$  values were calculated from Appendix A, Appendix C, and the first line of Table III. The xenon values were calculated with the last line of Table III and then reduced by 2.9%. This latter adjustment reflects the assessment of Table IV that our xenon noncritical viscosity data were more accurate ( $\pm 0.8\%$ ) than those from the capillary viscometer of Ref. 37.

<sup>1</sup>P. C. Hohenberg and B. I. Halperin, Rev. Mod. Phys. **49**, 435 (1977).

<sup>2</sup>J. V. Sengers, Int. J. Thermophys. **6**, 203 (1985).

<sup>3</sup>R. F. Berg and M. R. Moldover, J. Chem. Phys. **89**, 3694 (1988).

<sup>4</sup>J. K. Bhattarjee and R. A. Ferrell, Phys. Rev. A **28**, 2363 (1983).

<sup>5</sup>M. R. Moldover, J. V. Sengers, R. W. Gammon, and R. J. Hocken, Rev. Mod. Phys. **51**, 79 (1979).

<sup>6</sup>H. L. Swinney and D. L. Henry, Phys. Rev. A **8**, 2586 (1973).

<sup>7</sup>J. V. Sengers, in *Transport Phenomena—1973*, edited by J. Kestin, AIP Conf. Proc. No. 11 (American Institute of Physics, New York, 1973), p. 229.

<sup>8</sup>K. Kawasaki, Ann. Phys. (New York) **61**, 1 (1970).

<sup>9</sup>R. Perl and R. A. Ferrell, Phys. Rev. Lett. **29**, 51 (1972); Phys. Rev. A **6**, 358 (1972).

<sup>10</sup>T. Ohta, J. Phys. C **10**, 791 (1977).

<sup>11</sup>See review by J. V. Sengers, in *Recent Advances in Engineering Science, Vol. III*, edited by A. C. Eringen (Gordon and Breach, New York, 1968), p. 153.

<sup>12</sup>J. K. Bhattarjee, R. A. Ferrell, R. S. Basu, and J. V. Sengers, Phys. Rev. A **24**, 1469 (1981).

<sup>13</sup>G. A. Olchowy, Ph. D. thesis, University of Maryland (1989).

<sup>14</sup>G. A. Olchowy and J. V. Sengers, Phys. Rev. Lett. **61**, 15 (1988).

<sup>15</sup>G. A. Olchowy (private communication).

<sup>16</sup>R. F. Berg and M. R. Moldover, Rev. Sci. Instrum. **57**, 1667 (1986).

<sup>17</sup>R. F. Berg and M. R. Moldover, report to NASA Lewis Research Center (April 1989).

<sup>18</sup>L. Bruschi and G. Torzo, Phys. Lett. A **98**, 265 (1983).

<sup>19</sup>C. C. Agosta, S. Wang, L. H. Cohen, and H. Meyer, J. Low Temp. Phys. **67**, 237 (1987).

<sup>20</sup>D. Dahl and M. R. Moldover, Phys. Rev. A **6**, 1915 (1972).

<sup>21</sup>K. Nitsche and J. Straub, in *Proceedings of the 6th European Symposium on Material Sciences under Microgravity Conditions*, Bordeaux, France, 2–5 December 1986 (ESA, Paris, 1987), ESA spp-256, p. 109.

<sup>22</sup>A. Onuki, M. Mau, and R. A. Ferrell, Phys. Rev. A **41**, 2256 (1990).

<sup>23</sup>H. Boukari, J. N. Shaumeyer, M. E. Briggs, and R. W. Gammon, Phys. Rev. A **41**, 2260 (1990).

<sup>24</sup>B. Zappoli, D. Bailly, Y. Garrobo, B. Le Neindre, P. Guenon, and D. Beysens, Phys. Rev. A **41**, 2264 (1990).

<sup>25</sup>R. W. Gammon and J. N. Shaumeyer, "Science Requirements Document for Zeno," report to NASA Lewis Research Center (April 1988).

<sup>26</sup>MG Industries, 2460 Boulevard of the Generals, Valley Forge, PA 19482. Identification of brands does not imply endorsement by NIST.

<sup>27</sup>Matheson Gas Products, 30 Seaview Drive, Secaucus, NJ 07096.

<sup>28</sup>M. R. Moldover, J. Chem. Phys. **61**, 1766 (1974).

<sup>29</sup>U. Narger and D. A. Balzarini (private communication, 1989).

<sup>30</sup>L. D. Landau and E. M. Lifshitz, *Fluid Mechanics* (Pergamon, New York, 1959).

<sup>31</sup>J. Kestin and G. F. Newell, Z. Angew. Math. Phys. **8**, 433 (1957); D. A. Beckwith and G. F. Newell, *ibid.* **8**, 450 (1957).

<sup>32</sup>J. M. Grouvel and J. Kestin, Appl. Sci. Res. **34**, 427 (1978) [note that second term of Eq. (24) should use  $(6 + 16R/\pi h)$ ]; see also J. C. Nieuwoudt and J. V. Sengers, Physica **149A**, 107 (1988).

<sup>33</sup>J. Kestin, S. T. Ro, and W. A. Wakeham, J. Chem. Phys. **56**, 4114 (1972).

<sup>34</sup>J. Kestin, S. T. Ro, and W. A. Wakeham, J. Chem. Phys. **56**, 4119 (1972); J. Kestin, Phys. Chem. Earth **13-14**, Nobel Symposium, 295 (1982).

<sup>35</sup>H. Iwasaki and M. Takahashi, J. Chem. Phys. **74**, 1930 (1981).

<sup>36</sup>J. A. Jossi, L. I. Stiel, and G. Thodos, A.I.Ch.E. J. **8**, 59 (1962).

<sup>37</sup>E. G. Reynes and G. Thodos, Physica **30**, 1529 (1964).

<sup>38</sup>S. L. Rivkin, A. Ya. Levin, L. B. Izrailevskii, and K. G. Kharitonov, in *Proceedings of the 6th International Conference on the Properties of Steam*, edited by P. Bury, H. Perdon, and B. Vodaar (Editions Europ ennes Thermiques et Industries, Paris, 1975), p. 153; re-analyzed by J. T. R. Watson, R. S. Basu, and J. V. Sengers, J. Phys. Chem. Ref. Data **9**, 1255 (1983).

<sup>39</sup>V. N. Zozulya and Yu. P. Blagoi, Sov. Phys. JETP. **39**, 99 (1974); see analysis by R. S. Basu and J. V. Sengers, J. Heat Transfer **101**, 3 (1979).

<sup>40</sup>H. Iwasaki and M. Takahashi, in *Proceedings of the 4th International Conference on High Pressure*, Kyoto, 1974, p. 523.

<sup>41</sup>H. J. Strumpf, A. F. Collings, and C. J. Pings, J. Chem. Phys. **60**, 3109 (1974).

<sup>42</sup>J. H. B. Hoogland and N. J. Trappeniers, in *Proceedings of the Eighth Symposium on Thermophysical Properties*, edited by J. V. Sengers (American Society of Mechanical Engineers, New York, 1981), p. 440.

<sup>43</sup>H. R. van den Berg, C. A. ten Seldam, and P. S. van der Gulik, Physica A (to be published).

<sup>44</sup>P. Calmettes, Phys. Rev. Lett. **39**, 1151 (1977).

<sup>45</sup>J. C. Nieuwoudt and J. V. Sengers, J. Chem. Phys. **90**, 457 (1989).

<sup>46</sup>J. K. Bhattarjee (private communication).

<sup>47</sup>H. C. Burstyn, J. V. Sengers, J. K. Bhattarjee, and R. A. Ferrell, Phys. Rev. A **28**, 1567 (1983).

<sup>48</sup>H. G ttinger and D. S. Cannell, Phys. Rev. A **22**, 285 (1980); D. S. Cannell, *ibid.* **12**, 225 (1975); J. H. Lunacek and D. S. Cannell, Phys. Rev. Lett. **27**, 841 (1971); D. Beysens, in *Phase Transitions Carg se 1980*, edited by M. L vy, J.-C. Le Guillou, and J. Zinn-Justin (Plenum, New York, 1982); J. G. Shanks, University of Maryland, Ph. D. thesis (1986).

<sup>49</sup>J. V. Sengers and J. M. H. Levelt Sengers, Ann. Rev. Phys. Chem. **37**, 189 (1986).

<sup>50</sup>A. Michels, J. V. Sengers, and P. S. van der Gulik, Physica **28**, 1216 (1962); see also Ref. 2.

<sup>51</sup>R. Tofeu, B. Le Neindre, and P. Bury, C. R. Acad. Sci. Paris B **273**, 113 (1971).

<sup>52</sup>T. Wassenaar, dissertation, University of Amsterdam (1952).

<sup>53</sup>J. T. Ho and J. D. Lister, Phys. Rev. B **2**, 4523 (1970).